White Matter Characterization with Diffusional Kurtosis Imaging

Els Fieremans[a,*], **Jens H. Jensen**[a,b], and **Joseph A. Helpern**[a,b,c,d]

[a] Center for Biomedical Imaging, Department of Radiology, New York University School of Medicine, New York, New York, USA.

[b] Department of Physiology and Neuroscience, New York University School of Medicine, New York, New York, USA.

[c] Department of Psychiatry, New York University School of Medicine, New York, New York, USA.

[d] Department of Radiology and Radiological Science, Medical University of South Carolina, Charleston. South Carolina, USA (present address)

Abstract

Diffusional kurtosis imaging (DKI) is a clinically feasible extension of diffusion tensor imaging that probes restricted water diffusion in biological tissues using magnetic resonance imaging. Here we provide a physically meaningful interpretation of DKI metrics in white matter regions consisting of more or less parallel aligned fiber bundles by modeling the tissue as two non-exchanging compartments, the intra-axonal space and extra-axonal space. For the *b*-values typically used in DKI, the diffusion in each compartment is assumed to be anisotropic Gaussian and characterized by a diffusion tensor. The principal parameters of interest for the model include the intra- and extra-axonal diffusion tensors, the axonal water fraction and the tortuosity of the extra-axonal space. A key feature is that these can be determined directly from the diffusion metrics conventionally obtained with DKI. For three healthy young adults, the model parameters are estimated from the DKI metrics and shown to be consistent with literature values. In addition, as a partial validation of this DKI-based approach, we demonstrate good agreement between the DKI-derived axonal water fraction and the slow diffusion water fraction obtained from standard biexponential fitting to high *b*-value diffusion data. Combining the proposed WM model with DKI provides a convenient method for the clinical assessment of white matter in health and disease and could potentially provide important information on neurodegenerative disorders.

Keywords

Diffusion; White Matter; MRI; kurtosis; axonal density; microstructure

1 Introduction

Diffusion weighted imaging (DWI) is a widely applied and clinically important MRI method used to measure the micron-scale displacement of water molecules in the brain. Diffusion on this length scale is very sensitive to the microstructure of neural tissue, being strongly

*Correspondence to: Els Fieremans, Department of Radiology, New York University School of Medicine, 660 First Avenue, 4th floor, New York, NY 10016. Els.Fieremans@nyumc.org; Tel.: (212) 263-3344; Fax: (212)263-7541..

affected by the number, orientation and permeability of barriers (e.g. myelin) and the presence of various cell types and organelles (e.g. neurons, dendrites, axons, neurofilaments and microtubules) (Beaulieu, 2002). Moreover, as the tissue microarchitecture is closely associated with function, DWI offers a unique and very powerful method to study brain pathology.

By far the most widely applied DWI technique to date is diffusion tensor imaging (DTI), in which the apparent diffusion tensor is estimated from the measurement of the apparent diffusion coefficient (ADC) along multiple directions (Basser et al., 1994). Several rotationally invariant diffusion metrics can be extracted from a DTI-analysis, including the mean diffusivity (MD) and the fractional anisotropy (FA), which are both popular markers of white matter (WM) integrity (Pierpaoli and Basser, 1996). In addition, DTI is also a commonly used method for fiber tractography, i.e. reconstructing the pathways of major WM fiber tracts through the brain (Basser et al., 2000). Although DTI is an important technique for investigating mechanisms of health and disease in brain WM (Thomason and Thompson, 2011), among its limitations are the inability of DTI-based fiber tractography to resolve fiber crossings, and the lack of specificity to histological features.

While DWI has the potential to fully characterize the water diffusion properties of the brain, it is well recognized that DTI yields only a fraction of the information potentially accessible with DWI, which is mainly due to the fact that DTI is based upon a Gaussian approximation of the diffusion displacement probability function. Non-Gaussian diffusion is readily observed in the brain when applying diffusion gradients such that the corresponding b-value (diffusion weighting) is significantly higher than the typical DTI b-value of 1000 s/mm^2 (Assaf and Cohen, 1998; Niendorf et al., 1996). The non-Gaussian diffusion effects in the brain are believed to arise from diffusion restricted by barriers, such as cell membranes and organelles, as well as the presence of distinct water compartments with differing diffusivities.

Several techniques for assessing non-Gaussian diffusion have been developed (Alexander et al., 2002; Jensen and Helpern, 2010; Liu et al., 2004; Maier et al., 2004; Tuch, 2004; Wedeen et al., 2005). Among them, diffusional kurtosis imaging (DKI) has been proposed as a minimal extension of DTI that enables the quantification of non-Gaussian diffusion through the estimation of the diffusional kurtosis, a quantitative measure of the non-Gaussianity of the diffusion process (Jensen et al., 2010; Jensen et al., 2005; Lu et al., 2006). A typical DKI-protocol for brain requires a maximum b-value of 2000 s/mm^2 and DWI measurements along a minimum of 15 different directions (Tabesh et al., 2010). Quantitative rotationally invariant diffusion metrics can be extracted from the DKI-analysis, such as the mean kurtosis (MK), radial kurtosis and axial kurtosis, that are of potential interest to the study of white and gray matter integrity. So far, DKI has shown promising preliminary results for several brain diseases including stroke (Jensen et al., 2010), attention-deficit hyperactivity disorder (ADHD) (Helpern et al., 2010), the staging of glioblastomas (Raab et al., 2010), as well as normal aging (Falangola et al., 2008). Additionally, DKI is potentially useful in tractography for resolving crossing fibers (Lazar et al., 2008). However, similar to DTI, DKI metrics of non-Gaussianity are pure diffusion measures and lack microstructural and pathological specificity. Furthermore, a clear explanation for the microscopic origin of the diffusional kurtosis in WM has not been previously given.

The extraction of cell properties and histological details of WM necessarily relies on biophysical modeling of the DWI signal, and on the subsequent interpretation of the model parameters in terms of intrinsic tissue properties. The most basic model used to analyze high b-value data is the biexponential model that is based on the assumption of two non-exchanging compartments: one exhibiting fast diffusion, and the other slow diffusion.

Despite good fits of the DWI signal, the original attempt to assign the two compartments to the intra- and extracellular space is still a subject of a debate (Assaf and Cohen, 1998; Clark and Le Bihan, 2000; Kiselev and Il'yasov, 2007; Maier et al., 2004; Mulkern et al., 2000; Niendorf et al., 1996). However, for the WM, assigning the highly restricted water diffusion inside the axons to the slow compartment and the less hindered diffusion in the extra-axonal space to the fast compartment has been justified experimentally (Assaf and Basser, 2005; Assaf and Cohen, 2000; Assaf et al., 2004) and theoretically (Fieremans et al., 2010b).

A number of advanced morphology-based models have been proposed to interpret DWI in brain WM. As an early and comprehensive model, Stanisz et al. represented bovine optic nerve tissue by three compartments formed by spherical glial cells, prolate ellipsoidal axons and the extracellular space. By using this analytical model, the compartment parameters, such as volume fractions, compartment size, membrane permeability and diffusivity, could be estimated for fixed tissue (Stanisz et al., 1997). The less elaborate CHARMED model (Assaf and Basser, 2005; Assaf et al., 2004) assumes two types of diffusion in the brain: restricted diffusion inside impermeable cylindrical axons and hindered diffusion in the extra-axonal space, allowing estimation of the compartment volume fractions and diffusivities for the human brain *in vivo*. In the framework of "Axcaliber", the CHARMED model was further developed to extract the axonal diameter distribution, which was evaluated *ex vivo* on pig spinal cord (Assaf et al., 2008) and *in vivo* in the corpus callosum of a rat (Barazany et al., 2009). A similar model of two non-exchanging compartments has been developed by Jespersen et al, wherein the restricted diffusion component arises from an angular distribution of narrow cylinders (representing the axons and dendrites), allowing one to estimate the compartment volume fractions and diffusivities, as well as the intra-voxel distribution of fiber orientations, as demonstrated in fixed brain tissue of the rat and baboon (Jespersen et al., 2010; Jespersen et al., 2007). Recently, Alexander et al. proposed a four-compartment brain WM model that allows the axon diameter and density to be derived, as illustrated in fixed monkey brain and *in vivo* human brain (Alexander et al., 2010).

To extract all the features of the models summarized above, DWI data are needed for several high *b*-values (i.e., b ≥ 3000 s/mm^2), multiple diffusion gradient directions and/or different diffusion times, which necessitates long scan times and limits the applicability of these models for most clinical studies. Alternatively, DKI is a clinically feasible technique with acquisition times only a few minutes longer than conventional DTI. However, as DKI metrics of non-Gaussianity are model-independent, they must be augmented with a tissue model to help interpret the physical meaning of any changes associated with disease processes.

In this work, we focus on WM regions consisting of more or less parallel aligned fiber bundles and propose a model of diffusion in the WM that is suitable for DKI analysis and provide a more meaningful physical interpretation of DKI diffusion metrics in WM. We first introduce the WM diffusion model of two non-exchanging compartments: the intra-axonal space, consisting of impermeable cylindrical axons (IAS), and the extra-axonal space (EAS). Next, we demonstrate how the diffusion in each compartment appears to be Gaussian for the *b*-values typically used in DKI and hence can be described by compartment-specific diffusion tensors. Combining this model with DKI provides analytical expressions for the intra- and extra-axonal diffusion tensors, and allows for quantification of the axonal water fraction (AWF) and of the tortuosity of the EAS. We use then the newly proposed model to characterize human brain WM *in vivo* and discuss the biological significance of the tissue parameters as derived using DKI. Finally, we compare the AWF obtained from DKI-analysis to the slow diffusion fraction obtained from conventional biexponential fitting to high *b*-value diffusion data.

2 Methods

In this section, we first describe the WM model, discuss the validity of its assumptions, and outline its relation to DKI. We then specify the datasets, imaging protocols and data processing needed to evaluate the derived WM parameters.

2.1 White Matter Diffusion Model for DKI

2.1.1 Model Description and Assumptions—In this work, we make the following two main assumptions about *in vivo* diffusion in brain WM:

  i. The WM consists of two non-exchanging compartments: the intra-axonal space (IAS) and extra-axonal space (EAS): The IAS is assumed to consist mainly of myelinated axons that are idealized as infinitely long cylinders (there may possibly also be a small contribution to the IAS from unmyelinated axons, dendrites or glial processes). The protons trapped in the myelin are MRI invisible for echo times (TE ~ 100 ms) used in a typical DWI-experiment given their short T_2 relaxation times (Mackay et al., 1994; Stanisz et al., 1999). The remainder of the WM is referred to as the extra-axonal space (EAS) and modeled as an effective medium (Fieremans et al., 2010b), assuming the glial cells are in fast exchange with the extracellular matrix. This assumption is supported by the fact that glial cells are known to be highly permeable (Arciénega et al., 2010; Nielsen et al., 1997) and also because restricted diffusion inside the glial cells would result in a slow diffusion component that is independent of the gradient direction, which has not been observed in the *in vivo* brain WM (Alexander et al., 2010; Assaf and Basser, 2005). The exchange between the IAS and EAS is neglected, as myelinated axons have a very low permeability (Meier et al., 2003).

  ii. The diffusion in both the EAS and IAS can be modeled by compartment specific diffusion tensors, whereby we implicitly assume that the diffusion appears to be Gaussian, but not necessarily unrestricted, in each individual compartment. This assumption is justifiable for the EAS at clinically relevant diffusion times and for straight axonal bundles. In general, its validity depends both on the direction distribution of axons, the diffusion time, and the maximum *b*-value considered in the DWI-analysis, as will be discussed in more detail in the next section 2.1.2.

Based on these assumptions, both the IAS and EAS are modeled by the corresponding compartmental diffusion tensors $\mathbf{D}_a$ and $\mathbf{D}_e$. The axonal water fraction (AWF), denoted by the symbol *f*, is the fraction of MRI visible water in the axons relative to the total visible water signal. The DWI signal intensity, *S*, in the direction **n**, as a function of the diffusion weighting, *b*, in such a system is then described by

$$S(b)/S(0) = f \exp\left(-b\mathbf{n}^T \mathbf{D}_a \mathbf{n}\right) + (1-f)\exp\left(-b\mathbf{n}^T \mathbf{D}_e \mathbf{n}\right).$$

(1)

Below, we first justify Eq. (1) and then outline the procedure to extract the WM parameters based on the DKI representation of the DWI signal.

2.1.2 Model Justification—We substantiate here the assumption made in Eq. (1) of Gaussian diffusion in the EAS and the IAS. For the EAS, the mean square displacement of water molecules during a typical DWI experiment

$(\sim \sqrt{2D_e t} \approx \sqrt{2 \cdot 2\mu m^2/ms \cdot 50ms} = 14 \quad \mu m$, where D_e is the free extra-axonal diffusivity) is much greater than the correlation length of the axonal packing (~1 μm), so that the tortuosity asymptote is reached (Fieremans et al., 2010b). Hence, it is reasonable to assume

that the diffusion profile in the EAS at long times, while anisotropic, is Gaussian in every direction and can be represented by the diffusion tensor $\mathbf{D}_e$.

The diffusion in the IAS is highly restricted and in general non-Gaussian. However, the fact that there is no observed time dependence of the diffusion metrics at clinically available diffusion times (Clark et al., 2001) indicates that any effects of non-Gaussian diffusion due to barriers become negligible in the direction along the axons at long diffusion times. It is then reasonable to assume Gaussian diffusion in the intra-axonal compartment for a voxel consisting of perfectly aligned axons with zero radius as the transverse diffusivity is zero in this limit (Fieremans et al., 2010b). Hence, the DWI signal $S_\parallel$ becomes trivially Gaussian in all directions and is described by

$$\frac{S_\parallel(b)}{S_\parallel(0)}=\exp\left(-bD_a\cos^2\theta\right),$$

(2)

where D_a is the free intra-axonal diffusivity and θ is the angle with respect to the axon axis. The zero radius approximation is valid for long diffusion times $t \gg R^2/D_a$, where R is the axon radius. For typical values, $R \approx 1$ μm and $D_a \approx 1$ μm^2/ms, we find $t \gg 1$ ms, which is well satisfied for clinical DWI experiments, where $t \sim 50$ms.

When the axons are not perfectly aligned within a voxel, Gaussianity becomes dependent on both the direction distribution of the axons and the b-value. A general criterion for the diffusion to appear Gaussian in a given direction can be derived based on the cumulant expansion (Jensen et al., 2005; Kiselev, 2010),

$$\frac{S(b)}{S(0)}=\exp\left(-bD+\frac{1}{6}b^2D^2K+O\left(b^3\right)\right),$$

(3)

where S is the DWI signal and D, K are the apparent diffusion coefficient and diffusional kurtosis in that direction.

Whereas for the EAS and the case of perfectly aligned axons described earlier, the higher order cumulants vanish due to zero K or D, this is not necessarily true for any axonal geometry. To a good approximation, a compartment will appear Gaussian if the b-value

$$b \ll \frac{6}{DK},$$

(4)

so that the 2nd and (presumably) higher order terms in b become negligible in Eq. (3). As a practical matter, we adopt the criterion

$$b \leq \frac{1}{DK},$$

(5)

as the condition for being effectively Gaussian. This criterion can be used as a guide to whether the diffusion appears Gaussian in a specific axonal geometry for a given b-value.

As an example, consider a voxel that contains two crossing fiber bundles with equal volume fractions, oriented at polar angles (θ_A,θ_B) relative to a particular diffusion direction of interest, as illustrated in Fig. 1 (a). For such a system, D and K for the axonal compartment

can be analytically derived (see Appendix A) and the *b*-value condition for Gaussianity (5) can then be written as

$$bD_a \leq \frac{2}{3} \cdot \frac{\cos^2(\theta_A) + \cos^2(\theta_B)}{[\cos^2(\theta_A) - \cos^2(\theta_B)]^2},$$

(6)

where D_a is the free intra-axonal diffusivity. This condition is evaluated numerically in Fig. 1 (b), showing a substantial region of approximate Gaussianity in (θ_A, θ_B) space. In particular, for two axonal bundles intersecting at an angle ≤ 30 degrees, this axonal geometry will look essentially Gaussian for a typical DKI protocol (i.e., a maximum *b*-value of 2000 s/mm^2) *in all directions*. However, this axonal geometry may not necessarily be accurately modeled as a Gaussian compartment for higher *b*-values.

In the more general case of a voxel containing axon bundles that intersect at larger angles or for randomly oriented axons in a plane, the diffusion in such geometries will not be Gaussian anymore in all directions. Yet, the derivation in Appendix A illustrates that an approximately coplanar axonal geometry with an out of plane angular spread of up to ± 45° will, for a typical DKI protocol, be effectively Gaussian for diffusion in the direction perpendicular to the plane.

2.1.3 Model Parameters—Directly fitting the DWI signal for many directions simultaneously to Eq. (1) is a hard multi-parameter non-linear problem, whose solution is numerically challenging and may in practice be unstable to noise. An alternative, based on the biexponential fitting for each diffusion direction separately (Maier et al., 2004), has been shown to require high b-values which are typically above those utilized clinically (Kiselev and Il'yasov, 2007). Here we suggest utilizing the DKI metrics, which are determined by a straightforward linear fitting procedure, together with a set of relationships that connect these to the AWF and the tensors $\mathbf{D}_a$ and $\mathbf{D}_e$. In what follows next, we provide analytical expressions for the AWF, $\mathbf{D}_a$ and $\mathbf{D}_e$ based on the diffusion and kurtosis tensor. A detailed derivation is given in Appendix B.

2.1.3.1 Estimation of the Axonal Water Fraction: On a voxel-by-voxel basis, the AWF is estimated by

$$f_{K_{max}} = \frac{K_{max}}{K_{max}+3},$$

(7)

where K_{max} is the maximum kurtosis over *all* diffusion directions (based on the kurtosis tensor). Eq. (7) assumes there is a direction for which the IAS diffusivity $D_{a,i}=0$, while for the other directions the diffusion in the IAS appears Gaussian, according to criterion (5). This approximation for the AWF has a broad applicability, e.g. the derivation in Appendix A illustrates that in a quasi-coplanar axonal geometry the kurtosis as measured in the direction perpendicular to the fiber plane is typically the maximum kurtosis and thus indicates the water fraction of the restricted compartment.

When the assumption of above ($D_{a,i}=0$) is not precisely met (e.g. imperfect alignment of the axons or due to effects of finite axonal radius relative to the diffusion length), Eq. (7) becomes a lower bound for the AWF. In that case, a more accurate estimate of the AWF is given by

$$f_{D_a} = \frac{K_{max}}{K_{max} + 3\left(1 - \frac{\sqrt{K_{max}}(D_a - D_{a,min})}{D_1 \sqrt{K_1} + D_2 \sqrt{K_2} + D_3 \sqrt{K_3}}\right)^2},$$

(8)

where D_1, D_2, D_3 are the diffusion coefficients and K_1, K_2, K_3 the corresponding kurtoses along the axis directions of a chosen reference frame. We note that the term $D_1 \sqrt{K_1} + D_2 \sqrt{K_2} + D_3 \sqrt{K_3}$ is rotationally invariant as discussed in Appendix B. D_a is the axonal diffusion coefficient with $D_{a,min}$ being a lower bound for D_a, defined by:

$$D_{a,min} = 3\,\bar{D} - \frac{D_1 \sqrt{K_1} + D_2 \sqrt{K_2} + D_3 \sqrt{K_3}}{\sqrt{K_{max}}}.$$

(9)

D_a can then be estimated by selecting the maximum $D_{a,min}$ over all voxels within a specified region of interest (ROI). This estimate will be exact if the ROI contains at least one voxel wherein $D_{a,i}=0$ in a certain direction. This procedure assumes that D_a is the same for all the voxels within the ROI.

Alternatively, the AWF can be found from a conventional biexponential fit to high b-value diffusion data, as in many previous studies (Inglis et al., 2001; Maier et al., 2004; Mulkern et al., 2000; Niendorf et al., 1996), which will be performed in this study to evaluate our proposed WM model parameter estimates based on DKI metrics. The biexponential fitting approach requires, in practice, much higher maximum b-values than DKI (7000 s/mm^2 rather than 2000 s/mm^2), and hence, according to criterion (5), is only applicable in regions with nearly aligned fiber directions.

2.1.3.2 Estimation of the Compartment diffusivities: With an estimate for the AWF, given by Eq. (7) or (8), the IAS and EAS compartment diffusion coefficients in a given direction, $D_{a,i}$ and $D_{e,i}$, can be derived from the diffusion coefficient D_i and kurtosis K_i in that direction by:

$$D_{e,i} = D_i \left[1 + \sqrt{\frac{K_i f}{3(1-f)}}\right],$$

(10)

$$D_{a,i} = D_i \left[1 - \sqrt{\frac{K_i(1-f)}{3f}}\right].$$

(11)

We note that Eqs. (10) and (11) have the underlying assumption that $D_{a,i} \leq D_{e,i}$, which is justified by the arguments described in Appendix B and Fig. B.1(a-b). It also follows from Appendix B and Fig. B.1(c) that Eqs. (10) and (11) are true in *any* direction. Hence, by choosing 6 or more independent directions, we can then reconstruct (using the standard DTI method) the full diffusion tensors $\mathbf{D}_a$ and $\mathbf{D}_e$.

By applying this WM model to the DKI metrics, several compartment-specific metrics can be derived, in addition to the usual DTI/DKI parameters. The same rotationally invariant measures as derived in standard DTI can now be obtained specifically for each compartment tensor. For this study, we focus on the following WM metrics of interest:

- the axonal water fraction (AWF) as given by Eq. (7) or Eq. (8),

    - the intra−axonal diffusivity, $\quad D_a = \mathrm{tr}(\mathbf{D}_a)$,   (12)

- the axial EAS diffusivity, $\quad D_{e,\parallel} = \lambda_{e,1}$, $\quad$ where $\quad \lambda_{e,1}$ $\quad$ is the primary eigenvalue of $\quad \mathbf{D}_e$,   (13)

    - the radial EAS diffusivity, $\quad D_{e,\perp}$
      $= \dfrac{\lambda_{e,2} + \lambda_{e,3}}{2}$, $\quad$ where $\quad \lambda_{e,2}$,
      $\lambda_{e,3}$ $\quad$ are the $\quad 2^{nd}$,
      3rd $\quad$ eigenvalue of $\quad \mathbf{D}_e$ $\quad$ respectively,   (14)

- the tortuosity of the EAS $\quad$ (Sen and Basser, $\quad$ 2005), $\quad \alpha = \dfrac{D_{e,\parallel}}{D_{e,\perp}}$.   (15)

All of these WM metrics assume that Eq. (1) is valid in the considered voxel, as discussed earlier in section 2.1.2. This implies that Eq. (12) is a good approximation for the intra-axonal along axis diffusivity in voxels that contain fiber bundles with an angular spread of less than 30 degrees. In addition, the definition of the tortuosity (Eq. 15) is only meaningful in the specific case of a voxel containing a single fiber direction so that $D_{e,\parallel}$ (Eq. 13) represents then the EAS diffusivity in the direction along the fibers and $D_{e,\perp}$ (Eq. 14) the EAS diffusivity perpendicular to the fibers.

In what follows, we will estimate and evaluate each of these WM parameters in healthy volunteers. For the AWF, we will compare the estimated values with the values obtained from a biexponential fit.

2.2 MRI 2.2.1 Subjects

Test data sets for evaluating the model come from three healthy human volunteers. Subject 1 is a 27 year old female, subject 2 is a 28 year old female, subject 3 is a 28 year old male. The subjects were scanned with informed consent obtained as approved by our Institutional Review Board.

2.2.2 Image Acquisition—MRI images were acquired using a 3T wide-bore Siemens Verio system (Siemens Medical Solutions, Erlangen, Germany) with a transmission body coil and a 12-channel head coil for reception.

Whole brain T_1-weighted magnetization-prepared rapid gradient echo (MPRAGE) images were acquired with TR = 2200 ms, TI = 1100 ms, TE = 2.3 ms, matrix = 256 x 256, FOV = 256×256 mm^2, slices per slab = 192, slice thickness = 1 mm, band width = 260 Hz/pixel in a total time of 4:30 min.

Diffusion-weighted images were acquired along 30 gradient directions for b = 0, 1000, 2000 s/mm^2 with a twice-refocused spin-echo (TRSE) echo planar imaging sequence (Reese et al., 2003) with TR = 8700 ms, TE = 96 ms (corresponding diffusion time ~ 50 ms), matrix = 82×82, FOV = 222×222 mm^2, 40 slices, slice thickness = 2.7 mm, no gap, NEX = 11 for

$b = 0$, NEX = 2 for $b = 1000, 2000$ s/mm^2, band width = 1355 Hz/pixel in a total time of 20 min.

Additional DWIs were acquired along one direction for 16 b-values (0, 100, 500 to 7000 in increments of 500 s/mm^2). The gradient direction was the same as the direction of the slice selection, which was chosen perpendicular to the anterior commissure-posterior commissure (AC-PC) plane. A standard Stejskal-Tanner (Tanner and Stejskal, 1968) sequence was used instead of the TRSE diffusion preparation to minimize the echo time (TE = 132 ms) and repetition time (TR = 12,500 ms) in order to obtain a higher SNR and shorter scan time, respectively. Other imaging parameters were: matrix = 104×104, FOV = 280×280 mm^2, 40 slices, slice thickness = 2.7 mm, no gap, NEX = 8 for all b-values, band width = 1502 Hz/pixel. The total acquisition time was 36 min.

2.3 Analysis of the MRI data

2.3.1 Data Preprocessing—
Data preprocessing with SPM8 (Statistical Parametric Mapping, Wellcome Department of Imaging Neuroscience, University College London, UK) included 3D motion correction by aligning all DWIs to the first $b = 0$- image and removing cerebrospinal fluid (CSF) from the DWIs by applying a binary mask derived from thresholding the CSF probability map (created with SPM from segmentation of the $b = 0$ image) at a cut-off probability value of ≤ 0.2.

2.3.2 Voxelwise analysis—
The co-registered and masked DWI images acquired in 30 directions for $b = 0, 1000, 2000$ s/mm^2 were then further processed using in-house software (Diffusional Kurtosis Estimator (DKE) (Tabesh et al., 2010)) running in Matlab and the diffusion and kurtosis tensors were calculated on a voxel-by-voxel basis using a weighted linear least squares (LLS) fitting algorithm. The AWF was derived based on Eq. (7) where K_{max} is taken as the maximum value of calculated kurtosis-values along 10,000 randomly chosen directions based on the kurtosis tensor. The generated f-map, together with the diffusion and kurtosis tensor element maps were then used to derive parametric maps of the diffusion coefficients of the axonal and extra-axonal tensors $\mathbf{D}_a$ and $\mathbf{D}_e$ along the same 30 directions that were used for the DWI acquisition based on Eqs. (10) and (11). Next, the eigenvalues of $\mathbf{D}_a$ and $\mathbf{D}_e$ were obtained using the standard DTI method (Basser et al., 1994) and the specific WM parameters of interest D_a, $D_{e,\parallel}$, $D_{e,\perp}$ and α were derived based on Eqs. (12)-(15).

The idealized WM model described above assumes that the axons are more or less parallel and becomes less appropriate in regions of complex fiber architecture such as fiber crossings of significant fanning. Additionally, to justify the use of a biexponential fit to the signal decay averaged over an ROI (see further in section 2.3.3), precise unidirectionality of the fibers in the specific ROI is required. Therefore we limit this study to voxels in which a single fiber orientation is expected corresponding to straight parallel fibers. We computed the coefficients of linearity $c_L = \frac{\lambda_1 - \lambda_2}{\lambda_1}$, planarity $c_P = \frac{\lambda_2 - \lambda_3}{\lambda_1}$, and sphericity $c_S = \frac{\lambda_3}{\lambda_1}$, where $\lambda_1, \lambda_2,$ and λ_3 are the eigenvalues of the overall diffusion tensor $\mathbf{D}$ ($\lambda_1 \leq \lambda_2 \leq \lambda_3$), that describe how close $\mathbf{D}$ is to the generic cases of line, plane and sphere (Westin et al., 1999). For further processing we included only voxels that fulfilled

$$c_L \geq 0.4, c_P \leq 0.2, c_S \leq 0.35. \tag{16}$$

For each WM parameter, given by Eqs. (12)-(15), we derived the histogram, mean value and standard deviation over all voxels that fulfill criterion (16).

2.3.3 Biexponential fitting—Fiber bundles oriented in a plane perpendicular to the slice direction were identified for further analysis. ROIs were drawn on the color-coded FA map considering only voxels that are colored in red (left-right direction) and/or green (anterior-posterior direction). In addition, ROIs for which the mean values of c_L, c_P and c_S did not fulfill criterion (16) were excluded. ROIs meeting the criteria described above were the genu, midbody and splenium of the corpus callosum and selected parts of the left and right part of forceps major (*fmajor*) and the inferior fronto-occipital fasciculus (*ifo*).

For each ROI and *b*-value ($b = 0 – 7000$ s/mm^2), the signal of the DWIs acquired along the slice direction was averaged. The mean signal $S(b)$ was fitted by a biexponential function

$$S(b) = f_{\text{biexp}} e^{-bD_s} + \left(1 - f_{\text{biexp}}\right) e^{-bD_f},$$

(17)

with $D_s \leq D_f$. The fitting procedure was performed in Matlab using the trust region algorithm with the robust option set to bisquare, enabling a fit that minimizes the summed square of residuals, and down-weights outliers using bi-square weights. The fitted slow and fast diffusion coefficients, D_s and D_f, are then compared to the compartment diffusivities along the slice direction, $D_{a,\text{slice}}$ and $D_{e,\text{slice}}$. Similarly, the fraction f_{biexp} corresponding to D_s is compared to the AWF of our DKI WM model. The AWFs in the voxels of each ROI were estimated by either Eq. (7), or by Eq. (8) where D_a is selected as the maximum $D_{a,\text{min}}$ over the whole ROI. To reduce the effect of noise, the maximum $D_{a,\text{min}}$ was approximated as $\max(D_{a,\text{min}}) \approx \text{mean}(D_{a,\text{min}}) + \text{SD}(D_{a,\text{min}})$, where SD is the standard deviation over the whole ROI.

3 Results

This section shows the results of testing the new WM DKI model; first we evaluate the parametric maps of three healthy young adults, then we show the comparison between the DKI-derived AWF and the slow diffusion fraction as obtained from biexponential fitting in WM regions where the biexponential model is physically justified.

3.1 Voxelwise analysis

The low *b*-value diffusion data acquired over multiple directions were used for testing the DKI WM model. Parametric maps are shown in Fig. 2 for the WM metrics of interest (the AWF based on Eq. (7); the axonal diffusivity, D_a; the axial EAS diffusivity, $D_{e,\parallel}$; the radial EAS diffusivity, $D_{e,\perp}$; and the tortuosity of the EAS, α) for an axial slice through the genu and splenium of the corpus callosum of one subject. The AWF is highest in the splenium of the corpus callosum. The IAS diffusivity D_a is found to be smaller than the axial EAS diffusivity $D_{e,\parallel}$, and both are observed to be the highest in the corpus callosum (~1.2 μm^2/ms and ~ 2.5 μm^2/ms respectively), while the radial EAS diffusivity $D_{e,\perp}$ is found to be slightly lower in those regions. Consequently, the tortuosity of the EAS, as defined by Eqn. (15), is the highest in these regions of the corpus callosum.

The WM parameters are shown to be very reproducible between subjects. The histograms of the WM parameters of the same subject as in Fig. 2 are shown in Fig. 3. The parametric maps and histograms of the other two subjects appear to be very similar, which is demonstrated in Fig. 4, plotting the mean values and standard deviation of the WM parameters over all selected WM-voxels for each subject. Over all subjects, average values and standard deviations were found for the AWF, $f = 0.49 \pm 0.07$, the axonal diffusivity, $D_a = 0.99 \pm 0.18$, the axial EAS diffusivity, $D_{e,\parallel} = 2.26 \pm 0.31$, the radial EAS diffusivity, $D_{e,\perp} = 0.87 \pm 0.16$, and the tortuosity of the EAS, $\alpha = 2.75 \pm 1.13$.

For all the results shown in Figs. 2-4, only voxels were selected with a single fiber orientation according to criterion (16), which were respectively 19%, 18% and 24% of all WM voxels for the three subjects. In addition, a small number of voxels in the corpus callosum near the ventricles (< 0.3% of all WM voxels) was excluded from the analysis in which either D_3 is artifactually small (< 0.08 μm^2/ms) or $D_{e,\parallel}$ is artifactually high (> 3 μm^2/ms = diffusion coefficient of water at 37°C). To derive these ratios, a mask of all WM voxels was created based on the segmented MPRAGE-images (cut-off probability of ≤ 0.99) that were co-registered and resliced to the $b = 0$ – image.

3.2 Comparison to biexponential fit

The additional high b-value diffusion data acquired in the slice direction were used to compare the DKI WM model to the biexponential model. ROIs were chosen such that the voxels were in fiber bundles perpendicular to the diffusion gradient, i.e. the corpus callosum, the forceps major and parts of the inferior fronto-occipital fasciculus. The biexponential model, given by Eq. (17), fits the ROI-averaged b-dependent signal up to 7000 s/mm^2 very well for all ROIs (R^2 ≥ 0.997), as illustrated in Fig. 5 for one subject.

The theory predicts that the fitted slow and fast diffusion coefficient, D_s and D_f, correspond to the IAS and EAS compartment diffusivities in the slice direction, $D_{a,slice}$ and $D_{e,slice}$, respectively. The fitted slow diffusion coefficient D_s is on average 0.06 ± 0.02 μm^2/ms, whereas the fast diffusion coefficient D_f is on average 0.75 ± 0.17 μm^2/ms over all selected ROIs. As a comparison, $D_{a,slice}$ is on average 0.08 ± 0.02 μm^2/ms and $D_{e,slice}$ is on average 0.86 ± 0.15 μm^2/ms over the same ROIs as used in the biexponential analysis.

Similarly, the fraction f_{biexp} of the slow diffusion compartment in Eqn. (17) can also be compared to the AWF derived using our DKI WM model, approximated either by $f_{K_{max}}$ in Eq. (7) or by f_{D_a} in Eq. (8). To assess agreement between the parameters obtained from the biexponential model on the one hand and the DKI WM model on the other hand, Bland-Altman plots of the difference against their mean were created for each parameter set in Fig. 6 (Bland and Altman, 1986). The Bland-Altman plot for (D_s, $D_{a,slice}$) is plotted in Fig. 6(a), showing a mean bias of -0.03 μm^2/ms and lower and upper limits of agreement of - 0.12 μm^2/ms and 0.05 μm^2/ms. The Bland-Altman plot for (D_f, $D_{e,slice}$) is plotted in Fig. 6(b), showing a mean bias of 0.22 μm^2/ms and lower and upper limits of agreement of -0.05 μm^2/ms and 0.49 μm^2/ms. The Bland-Altman plot for (f_{biexp}, $f_{K_{max}}$) is plotted in Fig. 6(c), showing a mean bias of 0.05 and lower and upper limits of agreement of -0.02 and 0.12, and the Bland-Altman plot for (f_{biexp}, f_{D_a}) is plotted in Fig. 6(d), showing a mean bias of 0.01 and lower and upper limits of agreement of -0.04 and 0.07.

4 Discussion

DKI has been introduced as a clinically feasible technique to study restricted diffusion in brain WM (Jensen and Helpern, 2010; Jensen et al., 2005). It is a fast and robust method that quantifies the diffusion coefficient and diffusional kurtosis, both physically well-defined, model independent, diffusion metrics. In this work, we provide a physical interpretation for the diffusional kurtosis by augmenting the DKI metrics with an idealized model for WM tissue, as described in detail in section 2.1.1. The WM is modeled here by two non-exchanging compartments, the IAS and the EAS, as captured by Eq. (1). Similar multi-compartment models based on the IAS and EAS are commonly used with high b-valuediffusion data in brain WM (Alexander et al., 2010; Assaf et al., 2004; Jespersen et al., 2007; Sen and Basser, 2005) and are shown to explain simulated and experimental data very well (Fieremans et al., 2010b; Panagiotaki et al., 2009). We also note that other bi- and multiexponential models have been proposed that take a form similar to Eq. (1), but model

the diffusion originating purely from the IAS consisting of multiple fiber orientations (Anderson, 2005).

Fitting Eq.(1) directly to the raw diffusion data is a hard non-linear problem that has, to our knowledge, not been attempted and would likely be confounded by multiple local minima in the parameter space. We provide here a straightforward and practical method to solve Eq. (1) by utilizing the DKI metrics. In addition, our DKI-approach facilitates selecting the one solution as being the most physically reasonable, as the derivation in appendix B shows how the extra information contained in the kurtosis tensor allows one to resolve the sign ambiguity of Eq. (B3 - B4) and conclude that $D_{e,i} \geq D_{a,i}$.

Applying model (1) to *in vivo* human WM DKI data yields estimates of the AWF and the compartment-specific diffusion tensors, from which scalar parameters of potential interest can be derived, such as the radial and axial intra- and extra-axonal diffusivities and the tortuosity of the EAS. All these parameters values are consistent between subjects (Fig. 4) and agree with prior studies as discussed below in more detail. We also discuss how this approach can be useful in clinical applications, and finally we address some potential limitations.

4.1 Model Parameters

The axial compartment diffusivities, D_a and $D_{e,\parallel}$, provide estimates for the intrinsic intra- and extra-axonal diffusion coefficient of water in human WM. The axial diffusion is found to be higher in the EAS than in the IAS, which follows from Appendix B and is illustrated in Fig. B.1. This observation can be understood by the presence of cytoplasm and organelles in the IAS that plausibly slows down the diffusion. A similar experimental finding has been reported in fixed rat brain WM (Jespersen et al., 2010), in which a two-compartment model was used to interpret the high *b*-value diffusion data.

The best estimate for the "free" intra- and extra-axonal diffusion coefficients of water in human WM are probably the values of D_a and $D_{e,\parallel}$ in those voxels of the corpus callosum with the strongest fiber alignment. The IAS diffusion coefficient D_a is then about 1.2 μm^2/ms, resulting in 0.4 for the ratio of D_a relative to the free diffusion constant of water at 37°C. Remarkably, Kroenke et al. (2004) obtained the same ratio for the *in vivo* measured parallel diffusion coefficient of NAA in the corpus callosum relative to its diffusion coefficient in dilute aqeous solution. That study also reports a higher ratio of 0.46 as measured in large voxels within rat brains. Differences might be due to imperfect fiber alignment within the voxel, and/or the fact that NAA diffuses much slower than water (0.36 μm^2/ms versus 1.2 μm^2/ms). As a result, NAA has a shorter diffusion length (6 μm) than water (11 μm), and its diffusion is thus less hindered by intra-axonal restrictions such as axonal varicosities, that have an overall mean spacing of 5.2 μm (Shepherd and Raastad, 2003). The IAS diffusivity in the direction perpendicular to the fibers, $D_{a,slice}$, is found to be almost zero, which supports the assumption that the diffusion in the IAS is almost fully restricted.

The axial EAS diffusion coefficient in the corpus callosum is about 2.5 μm^2/ms, which is 17% lower than the free diffusion constant of water at 37°C (3 μm^2/ms), indicating that the water molecules are only weakly hindered by membranes in the EAS in the direction along the fibers. The radial EAS diffusivity, $D_{e,\perp}$, is found to be much smaller than $D_{e,\parallel}$, which supports the EAS diffusion in the direction perpendicular to the fibers being strongly restricted.

The EAS tortuosity provides an indirect measure of the myelinated axonal fraction (including the myelin), as it increases for decreasing EAS volume fraction (Fieremans et al., 2008). The higher tortuosity values observed in the corpus callosum (Fig. 2) can be

explained by the presence of myelin and a high axonal density. The mean value $\alpha = 2.79$ we found in this study for WM is close to literature values. As a comparison, a mean tortuosity value $\alpha = 3.1$ has been measured in brain extracellular space (Kroenke and Neil, 2004) using diffusion MRI. Similarly, a mean tortuosity value $\alpha = 2.89$ has been found for the corpus callosum of adult rat brain using the standard iontophoresis method with tetramethylammonium (TMA) as probing molecule (Syková and Nicholson, 2008) (this value is derived from the reported value of 1.7 for the tortuosity, operationally defined as $\sqrt{D_{\text{free}}/\text{ADC}}$, and squared according to our definition Eq. (15)).

The AWF provides a measure of the IAS water volume relative to the EAS water volume and neglects the myelin water that practically does not contribute to the DWI signal due to fast transverse relaxation. This parameter should not be confused with the total cellular volume fraction of approximately 0.8, as the EAS also contains glial cells. The highest AWF values are observed in the corpus callosum, as shown in Fig. 2 and Fig. 6, as expected. The mean value $f = 0.49$ we found in this study for WM is in good agreement with normalized water fractions as estimated using multiexponential analysis of T_1- and T_2-relaxation measurements in human WM (Hwang et al., 2010; Lancaster et al., 2003; Lancaster et al., 2005) and rat trigeminal nerve (Does and Gore, 2002). Our results confirm that in the WM there is no real disagreement between the fast and slow diffusion fractions from the biexponential fit and the physical water fractions of the EAS and IAS (Assaf and Basser, 2005; Maier et al., 2004).

When neglecting the contribution of the myelin volume, the measured AWF can be compared to histological volume fractions: Tang et al. (1997) performed stereology on human WM and found a mean value of 0.33 for the volume fraction of myelinated fibers. This value agrees well with the earlier reported mean AWF-value of 0.3 over all WM voxels with FA > 0.25 (Fieremans et al., 2010a). The mean AWF-value of 0.49 we report here is higher, probably because we limited this study to those WM-voxels (according to Eq. (16)) that have the highest fiber density. For example, the AWF-values we find in the corpus callosum (Fig. 6) compare favorably to the reported value of about 0.7 for the axonal volume density of the commisura anterior of rat brain based on AMG staining (Jespersen et al., 2010).

4.2 Comparison to the biexponential model

The values we find for the AWF using DKI data are also similar to the values found in other advanced multi-compartment models that typically require analysis of high *b*-value diffusion data (Alexander et al., 2010; Jespersen et al., 2010; Jespersen et al., 2007; Panagiotaki et al., 2009). We compared the DKI WM model here against the biexponential model using high *b*-value data. Assuming that the fraction of the slow diffusion component corresponds to the axonal compartment, we find a reasonable agreement between this fraction and the AWF. Although the agreement seems slightly better for the AWF based on an ROI estimate of D_a (Eq. (8)) in Fig. 6 (d), the voxel-based approach (Eq. (7)) in Fig. 6 (c) is more objective and easier to implement, while also providing a fairly good estimate. These preliminary results suggest that approximately the same information about compartment diffusivities and the AWF can be derived from DKI-data as from high *b*-value diffusion data using biexponential or more complicated fitting. The advantage of our approach is that the DKI data-acquisition time is much shorter because the DKI WM-analysis requires only low *b*-values (up to 2000 s/mm^2) and puts less demand on the hardware. Thanks to the relatively low *b*-value range, DKI also provides an adequate signal-to-noise (SNR) making the technique useful in a clinical setting.

Another potential advantage of the DKI WM model over other advanced high *b* diffusion models lies in the fact that because of the smaller *b*-range, the two-compartment model has a broader applicability in the case of voxels containing non-collinear axons. For the data analysis and ROI selection, we applied a mask that selected voxels with a homogeneous axon orientation (Eq. (16)). Whereas this mask is most likely a prerequisite for applying biexponential fitting using high *b*-value diffusion data, the derivation in section 2.1.1 (together with Fig. 1 and Appendix A) suggests that the DKI WM model might be valid in significantly more voxels than those selected by the WM mask. Future work will investigate in more detail the applicability of the DKI WM model in less highly oriented voxels.

4.3 Applications

This model offers new perspectives for the clinical assessment of WM tissue. DKI is relatively easy to implement on clinical scanners and a typical DKI protocol requires 7 to 20 minutes for full brain coverage depending on the hardware and imaging parameters (Jensen and Helpern, 2010; Tabesh et al., 2010). The current DKI WM model then allows for the estimation of various microstructural parameters from the DKI data, such as the compartment diffusivities and the water fractions of each compartment. The axonal water fraction is formally determined by the maximum kurtosis over all directions (Eq. (7)), but can in practice often be approximated by the radial kurtosis. The axial kurtosis reflects then the diffusional heterogeneity between the IAS and the EAS.

These parameters may help elucidate the meaning of changes in DKI metrics as observed in clinical studies. As an example, Jensen et al. (2010) reported substantial increases in the mean kurtosis within ischemic lesions for stroke patients. More specifically, for the lesions with strongly oriented axon bundles, the increase in the axial kurtosis was much greater than that in the radial kurtosis. Using our approach, it follows then naturally that this change is due to a large decrease of the intra-axonal diffusivity, as also suggested in their study. The AWF and the tortuosity are likely to be sensitive to changes in the number of axons, the myelin volume and axonal geometry and could potentially provide important information for assessing, e.g. multiple sclerosis (Inglese and Bester, 2010; Warlop et al., 2009; Warlop et al., 2008), Alzheimer's disease (Bartzokis), and other neuro-psychiatric and/or neuro-degenerative disorders that may be related to myelin dysfunction (Nave, 2010). More advanced analysis methods such as tract-based spatial statistics (TBSS) (Smith et al., 2006) and tractometry (Bells et al., 2011) seem particularly well suited for our model, as these naturally restrict the analysis to WM voxels consisting of strongly aligned fibers. Future work will focus on the clinical applications of the DKI WM model.

4.4 Limitations

The present WM model is highly idealized, with some aspects of water diffusion in WM not explicitly included. One such limitation is that the CSF is not considered as a separate compartment. A possible effect of different transverse relaxation times for the intra- and extra-axonal compartments is also neglected, that may influence the estimates of the AWF and the tortuosity (Frøhlich et al., 2008). Furthermore, the DKI WM model is based on relatively low *b*-values diffusion data in a small number of diffusion directions, which inherently limits the amount of information that can be extracted. This is in contrast to other advanced diffusion models, based on high *b*-value and/or many gradient directions, aiming to characterize the axon diameter, diameter distribution or fiber orientation distribution (Alexander et al., 2010; Assaf et al., 2008; Barazany et al., 2009; Jespersen et al., 2010). The limited information available in a DKI-dataset, due to its low *b*-value and limited angular information, makes it impossible to incorporate all of these as well as some other features into our model. Nonetheless, our proposed DKI WM model seems to be a useful description of the actual biophysical structure that yields realistic values for all microscopic parameter

values included in the model. Important advantages of our approach are both its simplicity and the practical benefits of only requiring relatively low *b*-value diffusion data.

5 Conclusion

We have proposed an idealized two-compartment no exchange diffusion model of white matter suitable for analysis with diffusional kurtosis imaging (DKI) diffusion metrics. Based on this model, standard DKI metrics can be used to estimate the intra- and extra-axonal diffusivities, the axonal water fraction, and the tortuosity of the extra-axonal geometry. Values for these parameters obtained in healthy young adults agree well with those of prior studies. The axonal water fraction and the tortuosity provide information related to axonal and myelin density, which may be useful in assessing myelin-associated neuropathologies. Since a DKI dataset can be acquired within a few minutes, this approach can be applied for the quantitative assessment of white matter tissue properties in a clinical setting.

Acknowledgments

Appendix A: Gaussianity condition for axonal bundles

The bundles of axons are regarded as Gaussian compartments in our DKI WM model. We propose criterion (5) to test the validity of this assumption. Here we apply this criterion for the two axonal compartment geometries discussed in section 2.1.1. For that, we derive expressions for the compartmental *D* and *K* in these systems.

The first example discussed in section 2.1.2 is a voxel consisting of two crossing fiber bundles, oriented at polar angles (θ_A, θ_B) relative to a particular diffusion direction of interest, as illustrated in Fig. 1 (a). When idealizing the axons as having zero radius, the total axonal diffusion coefficient in such a system is given by

$$D = \frac{D_a}{2} \left[\cos^2(\theta_A) + \cos^2(\theta_B) \right],$$

(A.1)

where we have assumed for simplicity the two bundles have the same water fractions and D_a is the free intra-axonal diffusivity. The kurtosis for a given direction is derived using the standard formula for the multiple compartment kurtosis (Jensen and Helpern, 2010):

$$K = 3 \frac{\left[\cos^2(\theta_A) - \cos^2(\theta_B) \right]^2}{\left[\cos^2(\theta_A) + \cos^2(\theta_B) \right]^2}.$$

(A.2)

Substituting Eqs. (A.1) and (A.2) in the *b*-value criterion for Gaussianity (5), yields Eq. (6) in section 2.1.2.

Next, we consider the general case of axons that are oriented according to a direction distribution of $F(\mathbf{n})$, where **n** is a unit vector parallel to a particular axon. The distribution of directions is normalized so that

$$1 = \int d\Omega_{\mathbf{n}} \, F(\mathbf{n}),$$

(A.3)

where $d\Omega_{\mathbf{n}}$ is a solid angle element and the integral is taken over all possible directions. The diffusion coefficient in a direction $\mathbf{n}$ is then given by

$$D(\mathbf{n}) = D_a \int d\Omega_{\mathbf{n}}, \; F(\mathbf{n}')(\mathbf{n} \cdot \mathbf{n}')^2,$$

(A.4)

and, similarly, the diffusional kurtosis is given by

$$K(\mathbf{n}) = 3 \left\{ \frac{\int d\Omega_{\mathbf{n}}, \; F(\mathbf{n}')(\mathbf{n} \cdot \mathbf{n}')^4}{\left[\int d\Omega_{\mathbf{n}}, \; F(\mathbf{n}')(\mathbf{n} \cdot \mathbf{n}')^2\right]^2} - 1 \right\}.$$

(A.5)

Now let us consider a spherical coordinate system with $\mathbf{n}$ corresponding to the z-axis. Then we have

$$D = D_a \int_0^\pi d\theta \sin(\theta) \, \cos^2(\theta) \, G(\theta),$$

(A.6)

where

$$G(\theta) \equiv \int_0^{2\pi} d\phi \, F(\theta, \phi),$$

(A.7)

with (θ, ϕ) being the usual spherical angles. Note that $G(\theta)$ is normalized so that

$$1 = \int_0^\pi d\theta \sin\theta \, G(\theta).$$

(A.8)

Now we consider the 2$^{\text{nd}}$ example of axons in a nearly coplanar configuration with the diffusion gradient applied perpendicular to the axons. Let us assume that the axons are uniformly distributed within a range of angles defined by

$$G(\theta) = \begin{cases} |2 \; \sin\theta_0|^{-1}, & \text{if } \frac{\pi}{2} - \theta_0 < \theta < \frac{\pi}{2} + \theta_0 \\ 0, & \text{otherwise} \end{cases}.$$

(A.9)

One may readily verify that the model of Eq. (A.9) satisfies the normalization condition of Eq. (A.8). Combining Eqs. (A.4)-(A.9) results in the compartment diffusivity and kurtosis:

$$D = \frac{D_a}{3} \sin^2 \, \theta_0,$$

(A.10)

and

$$K = \frac{12}{5},$$

(A.11)

independent of θ_0, which using criterion (5), leads to the b-value condition

$$b \leq \frac{5}{4D_a \sin^2 \theta_0}.$$

(A.12)

So even for a $\pi/2$-range ($\theta_0 = \pi/4$), taking $D_a = 1$ μm^2, we find $b \leq 2500$ s/mm^2, which is adequate for DKI.

Appendix B: Derivation of DKI WM parameters

Here we outline the derivations of some of the basic results presented in the section 2.1.3. To develop the DKI WM model, we choose an arbitrary reference frame where D_1, D_2, D_3 are the measured diffusion coefficients along the axis directions 1, 2 and 3 and K_1, K_2, K_3 the corresponding kurtoses. The diagonal elements of the compartmental diffusion tensors $\mathbf{D}_a$ and $\mathbf{D}_e$ in Eq. (1) in this basis are $D_{a,1}, D_{a,2}, D_{a,3}$ and $D_{e,1}, D_{e,2}, D_{e,3}$ respectively. By modeling the system as two non-exchanging compartments, the overall diffusion coefficients, D_1, D_2, D_3, can be described as a function of the model parameters:

$$D_i = f D_{a,i} + (1 - f) D_{e,i},$$

(B.1)

for i = 1, 2 and 3, where f is the volume fraction of the IAS.

Similarly, the along axis kurtoses, K_1, K_2 and K_3, are related to the model parameters by

$$K_i = 3f (1 - f) \frac{(D_{e,i} - D_{a,i})^2}{D_i^2},$$

(B.2)

for i = 1, 2 and 3.

With a given estimate for f, Eqs. (B.1) and (B.2) can be inverted resulting in:

$$D_{e,i} = D_i \left[1 \pm_i \sqrt{\frac{K_i f}{3 (1 - f)}} \right],$$

(B.3)

and

$$D_{a,i} = D_i \left[1 \mp_i \sqrt{\frac{K_i (1 - f)}{3f}} \right],$$

(B.4)

for i = 1, 2 and 3.

For the small axon approximation, one can show that

$$D_a = D_{a,1} + D_{a,2} + D_{a,3},$$

(B.5)

where D_a is the free longitudinal intra-axonal diffusion coefficient along the axis. In addition, the mean extra-axonal diffusivity is

$$\bar{D_e} \equiv \frac{1}{3} \left(D_{e,1} + D_{e,2} + D_{e,3} \right). \tag{B.6}$$

We first resolve the sign ambiguities in Eqs. (B.3) and (B.4) in the reference frame in which the overall **D** is diagonal: Taking $D_{e,3} \geq D_{a,3}$ makes physical sense since the 3$^{\rm rd}$ direction (which by assumption has the smallest diffusion coefficient) should be roughly perpendicular to the axon direction. Thus, we take the upper sign for the 3$^{\rm rd}$ direction. The signs for the 1$^{\rm st}$ and 2$^{\rm nd}$ directions are then determined by

$$\eta_i = \frac{1}{\sqrt{W_{iiii} W_{3333}}} \cdot \left(3 W_{ii33} - \frac{2 W_{i333}^2}{W_{3333}} \right), \tag{B.7}$$

which is, theoretically, 1 for the upper sign and –1 for the lower sign. In Eq. (B.7) W_{ijkl} is the kurtosis tensor, here defined in the frame of reference where the overall **D** is diagonal. The derivation of Eq. (B.7) follows from the properties of the kurtosis tensor as described by (Jensen et al., 2005; Lu et al., 2006) but is omitted due to length considerations. Empirically η_i is found to be about 1 for most voxels in healthy young brain, as illustrated in the example in Fig. B.1 (a) and (b). Hence, $D_{e,i} \geq D_{a,i}$ in the eigenframe in which the overall **D** is diagonal.

Next, we show that $D_{e,i} \geq D_{a,i}$ also holds in arbitrary frames as long as $K_{min} > 0$: From Eqs. (B.1), (B.5), and (B.6), we see that

$$\bar{D_e} = \frac{1}{3(1-f)} \cdot \left(3 \bar{D} - f D_a \right), \tag{B.8}$$

where $\bar{D} \equiv (D_1 + D_2 + D_3)/3$ the total mean diffusivity. Applying Eq. (B.2) leads to

$$\pm D_1 \sqrt{K_1} \pm D_2 \sqrt{K_2} \pm D_3 \sqrt{K_3} = \left(3 \bar{D_e} - D_a \right) \sqrt{3f(1-f)}, \tag{B.9}$$

Combining with Eq. (B.8) yields the following expression:

$$\pm D_1 \sqrt{K_1} \pm D_2 \sqrt{K_2} \pm D_3 \sqrt{K_3} = \left(3 \bar{D} - D_a \right) \sqrt{\frac{3f}{(1-f)}}. \tag{B.10}$$

Note that the right side of Eq. (B.10) is independent of the choice of reference frame. The same must then be true for the left side. Now let us assume that we start in the eigenframe of the overall **D** for which $\pm_i = +$ for $i = 1, 2, 3$ and imagine continuously rotating the reference frame so that the values for (D_1, D_2, D_3) and (K_1, K_2, K_3) also change continuously. For the left side, continuity implies that the sign ambiguity $\pm_i$ can only flip for a reference frame in which D_i and/or K_i vanish. For brain tissue, we know that D_i does not vanish, as all the diffusion tensor eigenvalues are positive. Thus, we can only have a sign flip if there is a diffusion direction for which K_i vanishes. As a corollary, we see that if $K_{min} > 0$, where K_{min} is the kurtosis minimum for all directions, then if the upper signs apply in one frame of reference then they must also apply in all reference frames. Empirically, K_{min} is found to be positive (> 0) for most voxels in healthy young brain white matter, as illustrated in the example in Fig. B.1 (c). Therefore, we take the upper in sign in Eqs. (B.3) and (B.4)

henceforth, so that $D_{e,i} \geq D_{a,i}$ in any frame of reference. With this preferred sign choice, Eqs. (B.3) and (B.4) can be rewritten as Eqs. (10) and (11) in section 2.1.3.2.

In order to derive expressions for f, we express first all the undetermined model parameters in Eqs. (B.1) and (B.2) via D_a, the free longitudinal intra-axonal diffusion coefficient along the axis, and then try to estimate D_a. According to our sign choice, solving Eq. (B.10) for f gives

$$f = \frac{\left(D_1 \sqrt{K_1} + D_2 \sqrt{K_2} + D_3 \sqrt{K_3}\right)^2}{\left(D_1 \sqrt{K_1} + D_2 \sqrt{K_2} + D_3 \sqrt{K_3}\right)^2 + 3\left(3 \bar{D} - D_a\right)^2}.$$

(B.11)

Thus the AWF can be found from the DKI measurements plus an estimate for D_a. What is left now is to estimate D_a. The physical requirement $D_{a,i} \geq 0$, combined with Eq. (B.4), yields the condition

$$K_i \leq \frac{3f}{(1-f)}.$$

(B.12)

Applying this to Eq. (B.10) leads to

$$D_1 \sqrt{K_1} + D_2 \sqrt{K_2} + D_3 \sqrt{K_3} \geq \left(3 \bar{D} - D_a\right) \sqrt{K_i},$$

(B.13)

We then have the lower bound of

$$D_a \geq 3 \bar{D} - \frac{D_1 \sqrt{K_1} + D_2 \sqrt{K_2} + D_3 \sqrt{K_3}}{\sqrt{K_i}} \equiv D_{a,\min}.$$

(B.14)

So the largest kurtosis value $K_i = K_{\max}$ in the denominator gives the best lower bound and hence the best estimate for D_a.

Now let us define

$$D'_a \equiv \text{maximum} \left(3 \bar{D} - \frac{D_1 \sqrt{K_1} + D_2 \sqrt{K_2} + D_3 \sqrt{K_3}}{\sqrt{K_{\max}}}\right),$$

(B.15)

where we vary the right hand side over all voxels within a specified ROI. We may then reasonably make the approximation $\bar{D}_a \approx \bar{D}'_a$. This would be exact if the axons are perfectly aligned in any of the voxels.

Eqs. (B.11) and (B.14) are equivalent to Eqs. (8) and (9) in section 2.1.3.1. For ROI consisting of a single voxel, Eq. (B.11) simplifies in combination with Eq. (B.15), resulting in Eq. (7).

Abbreviations

ADC   apparent diffusion coefficient

AWF	axonal water fraction
DTI	diffusion tensor imaging
DKI	diffusional kurtosis imaging
DWI	diffusion weighted imaging or diffusion weighted image
EAS	extra-axonal space
FA	fractional anisotropy
IAS	intra-axonal space
MD	mean diffusivity
MRI	magnetic resonance imaging
ROI	region of interest
SD	standard deviation
WM	white matter

References

Alexander DC, Barker GJ, Arridge SR. Detection and modeling of non-Gaussian apparent diffusion coefficient profiles in human brain data. Magnetic Resonance in Medicine. 2002; 48:331–340. [PubMed: 12210942]

Alexander DC, Hubbard PL, Hall MG, Moore EA, Ptito M, Parker GJM, Dyrby TB. Orientationally invariant indices of axon diameter and density from diffusion MRI. Neuroimage. 2010; 52:1374–1389. [PubMed: 20580932]

Anderson AW. Measurement of fiber orientation distributions using high angular resolution diffusion imaging. Magnetic Resonance in Medicine. 2005; 54:1194–1206. [PubMed: 16161109]

Arciénega II, Brunet JF, Bloch J, Badaut J. Cell locations for AQP1, AQP4 and 9 in the non-human primate brain. Neuroscience. 2010; 167:1103–1114. [PubMed: 20226845]

Assaf Y, Basser PJ. Composite hindered and restricted model of diffusion (CHARMED) MR imaging of the human brain. Neuroimage. 2005; 27:48–58. [PubMed: 15979342]

Assaf Y, Blumenfeld-Katzir T, Yovel Y, Basser PJ. Axcaliber: A method for measuring axon diameter distribution from diffusion MRI. Magnetic Resonance in Medicine. 2008; 59:1347–1354. [PubMed: 18506799]

Assaf Y, Cohen Y. Non-Mono-Exponential Attenuation of Water andN-Acetyl Aspartate Signals Due to Diffusion in Brain Tissue. Journal of Magnetic Resonance. 1998; 131:69–85. [PubMed: 9533908]

Assaf Y, Cohen Y. Assignment of the water slow-diffusing component in the central nervous system using q-space diffusion MRS: Implications for fiber tract imaging. Magnetic Resonance in Medicine. 2000; 43:191–199. [PubMed: 10680682]

Assaf Y, Freidlin RZ, Rohde GK, Basser PJ. New modeling and experimental framework to characterize hindered and restricted water diffusion in brain white matter. Magnetic Resonance in Medicine. 2004; 52:965–978. [PubMed: 15508168]

Bland MJ, Altman D. STATISTICAL METHODS FOR ASSESSING AGREEMENT BETWEEN TWO METHODS OF CLINICAL MEASUREMENT. The Lancet. 1986; 327:307–310.

Barazany D, Basser PJ, Assaf Y. In vivo measurement of axon diameter distribution in the corpus callosum of rat brain. Brain. 2009; 132:1210–1220. [PubMed: 19403788]

Bartzokis G. Alzheimer's disease as homeostatic responses to age-related myelin breakdown. Neurobiology of Aging. In Press, Corrected Proof.

Basser P, Pajevic S, Pierpaoli C, Duda J, Aldroubi A. In vivo fiber tractography using DT-MRI data. Magnetic Resonance in Medicine. 2000; 44:625–632. [PubMed: 11025519]

Basser PJ, Mattiello J, LeBihan D. Estimation of the effective self-diffusion tensor from the NMR spin echo. Journal of Magnetic Resonance. Series B. 1994; 103:247–254. [PubMed: 8019776]

Beaulieu C. The basis of anisotropic water diffusion in the nervous system - a technical review. NMR in Biomedicine. 2002; 15:435–455. [PubMed: 12489094]

Bells, S.; Cercignani, M.; Deoni, S.; Assaf, Y.; Pasternak, O.; Evans, CJ.; Leemans, A.; Jones, DK. Tractometry – Comprehensive Multi-modal Quantitative Assessment of White Matter Along Specific Tracts.. International Society for Magnetic Resonance in Medicine - 19th Scientific Meeting; Montreal, Canada. 2011. p. 678

Clark C, Hedehus M, Moseley M. Diffusion time dependence of the apparent diffusion tensor in healthy human brain and white matter disease. Magnetic Resonance in Medicine. 2001; 45:1126–1129. [PubMed: 11378893]

Clark CA, Le Bihan D. Water diffusion compartmentation and anisotropy at high b values in the human brain. Magnetic Resonance in Medicine. 2000; 44:852–859. [PubMed: 11108621]

Does MD, Gore JC. Compartmental study of T1 and T2 in rat brain and trigeminal nerve in vivo. Magnetic Resonance in Medicine. 2002; 47:274–283. [PubMed: 11810670]

Falangola MF, Jensen JH, Babb JS, Hu C, Castellanos FX, Di Martino A, Ferris SH, Helpern JA. Age-related non-Gaussian diffusion patterns in the prefrontal brain. Journal of Magnetic Resonance Imaging. 2008; 28:1345–1350. [PubMed: 19025941]

Fieremans E, Dedeene Y, Delputte S, Ozdemir M, Dasseler Y, Vlassenbroeck J, Deblaere K, Achten E, Lemahieu I. Simulation and experimental verification of the diffusion in an anisotropic fiber phantom. Journal of Magnetic Resonance. 2008; 190:189–199. [PubMed: 18023218]

Fieremans, E.; Jensen, J.; Tabesh, A.; Hu, C.; Helpern, J. White matter model for diffusional kurtosis imaging.. Proceedings of the 18th Annual Meeting of the International Society for Magnetic Resonance in Medicine; Stockholm, Sweden. 2010a. p. 1596

Fieremans E, Novikov DS, Jensen JH, Helpern JA. Monte Carlo study of a two-compartment exchange model of diffusion. NMR in Biomedicine. 2010b; 23:711–724. [PubMed: 20882537]

Frøhlich AF, Jespersen SN, Østergaard L, Kiselev VG. The effect of impermeable boundaries of arbitrary geometry on the apparent diffusion coefficient. Journal of Magnetic Resonance. 2008; 194:128–135. [PubMed: 18619878]

Helpern JA, Adisetiyo V, Falangola MF, Hu C, Di Martino A, Williams K, Castellanos FX, Jensen JH. Preliminary Evidence of Altered Gray and White Matter Microstructural Development in the Frontal Lobe of Adolescents With Attention-Deficit Hyperactivity Disorder: A Diffusional Kurtosis Imaging Study. Journal of Magnetic Resonance Imaging. 2010 in press.

Hwang D, Kim D-H, Du YP. In vivo multi-slice mapping of myelin water content using T2* decay. Neuroimage. 2010; 52:198–204. [PubMed: 20398770]

Inglese M, Bester M. Diffusion imaging in multiple sclerosis: research and clinical implications. NMR in Biomedicine. 2010; 23:865–872. [PubMed: 20882528]

Inglis BA, Bossart EL, Buckley DL, Wirth ED, Mareci TH. Visualization of neural tissue water compartments using biexponential diffusion tensor MRI. Magnetic Resonance in Medicine. 2001; 45:580–587. [PubMed: 11283985]

Jensen JH, Falangola MF, Hu C, Tabesh A, Rapalino O, Lo C, Helpern JA. Preliminary observations of increased diffusional kurtosis in human brain following recent cerebral infarction. NMR in Biomedicine. 2010 in press.

Jensen JH, Helpern JA. MRI quantification of non-Gaussian water diffusion by kurtosis analysis. NMR in Biomedicine. 2010; 23:698–710. [PubMed: 20632416]

Jensen JH, Helpern JA, Ramani A, Lu H, Kaczynski K. Diffusional kurtosis imaging: the quantification of non-gaussian water diffusion by means of magnetic resonance imaging. Magnetic Resonance in Medicine. 2005; 53:1432–1440. [PubMed: 15906300]

Jespersen SN, Bjarkam CR, Nyengaard JR, Chakravarty MM, Hansen B, Vosegaard T, Østergaard L, Yablonskiy D, Nielsen NC, Vestergaard-Poulsen P. Neurite density from magnetic resonance diffusion measurements at ultrahigh field: Comparison with light microscopy and electron microscopy. Neuroimage. 2010; 49:205–216. [PubMed: 19732836]

Jespersen SN, Kroenke CD, Østergaard L, Ackerman JJH, Yablonskiy DA. Modeling dendrite density from magnetic resonance diffusion measurements. Neuroimage. 2007; 34:1473–1486. [PubMed: 17188901]

Kiselev, V. The cumulant expansion: an overarching mathematical framework for understanding diffusion NMR.. In: Jones, DK., editor. Diffusion MRI: Theory, Methods and Applications. Oxford University Press; Oxford: 2011.

Kiselev V, Il'yasov K. Is the "biexponential diffusion" biexponential? Magnetic Resonance in Medicine. 2007; 57:464–469. [PubMed: 17326171]

Kroenke CD, Ackerman JJH, Yablonskiy DA. On the nature of the NAA diffusion attenuated MR signal in the central nervous system. Magn. Reson. Med. 2004; 52:1052–1059. [PubMed: 15508157]

Kroenke CD, Neil JJ. Use of magnetic resonance to measure molecular diffusion within the brain extracellular space. Neurochemistry International. 2004; 45:561–568. [PubMed: 15186923]

Lancaster JL, Andrews T, Hardies LJ, Dodd S, Fox PT. Three-pool model of white matter. Journal of Magnetic Resonance Imaging. 2003; 17:1–10. [PubMed: 12500269]

Lancaster JL, Cody JD, Andrews T, Hardies LJ, Hale DE, Fox PT. Myelination in Children with Partial Deletions of Chromosome 18q. AJNR. American Journal of Neuroradiology. 2005; 26:447–454. [PubMed: 15760848]

Lazar M, Jensen JH, Xuan L, Helpern JA. Estimation of the orientation distribution function from diffusional kurtosis imaging. Magnetic Resonance in Medicine. 2008; 60:774–781. [PubMed: 18816827]

Liu C, Bammer R, Acar B, Moseley ME. Characterizing non-gaussian diffusion by using generalized diffusion tensors. Magnetic Resonance in Medicine. 2004; 51:924–937. [PubMed: 15122674]

Lu H, Jensen JH, Ramani A, Helpern JA. Three-dimensional characterization of non-gaussian water diffusion in humans using diffusion kurtosis imaging. NMR in Biomedicine. 2006; 19:236–247. [PubMed: 16521095]

Mackay A, Whittall K, Adler J, Li D, Paty D, Graeb D. In vivo visualization of myelin water in brain by magnetic resonance. Magnetic Resonance in Medicine. 1994; 31:673–677. [PubMed: 8057820]

Maier SE, Vajapeyam S, Mamata H, Westin CF, Jolesz FA, Mulkern RV. Biexponential diffusion tensor analysis of human brain diffusion data. Magnetic Resonance in Medicine. 2004; 51:321–330. [PubMed: 14755658]

Meier C, Dreher W, Leibfritz D. Diffusion in compartmental systems. II. Diffusion-weighted measurements of rat brain tissue in vivo and postmortem at very large *b*-values. Magnetic Resonance in Medicine. 2003; 50:510–514. [PubMed: 12939758]

Mulkern RV, Zengingonul HP, Robertson RL, Bogner P, Zou KH, Gudbjartsson H, Guttmann CR, Holtzman D, Kyriakos W, Jolesz FA, Maier SE. Multi-component apparent diffusion coefficients in human brain: relationship to spin-lattice relaxation. Magnetic Resonance in Medicine. 2000; 44:292–300. [PubMed: 10918329]

Nave K-A. Myelination and support of axonal integrity by glia. Nature. 2010; 468:244–252. [PubMed: 21068833]

Nielsen S, Arnulf Nagelhus E, Amiry-Moghaddam M, Bourque C, Agre P, Petter Ottersen O. Specialized Membrane Domains for Water Transport in Glial Cells: High-Resolution Immunogold Cytochemistry of Aquaporin-4 in Rat Brain. Journal of Neuroscience. 1997; 17:171–180. [PubMed: 8987746]

Niendorf T, Dijkhuizen RM, Norris DG, van Lookeren Campagne M, Nicolay K. Biexponential diffusion attenuation in various states of brain tissue: implications for diffusion-weighted imaging. Magnetic Resonance in Medicine. 1996; 36:847–857. [PubMed: 8946350]

Panagiotaki E, Fonteijn H, Siow B, Hall M, Price A, Lythgoe M, Alexander D. Yang G-Z, Hawkes D, Rueckert D, Noble A, Taylor C. Two-Compartment Models of the Diffusion MR Signal in Brain White Matter. Medical Image Computing and Computer-Assisted Intervention – MICCAI 2009. Springer Berlin / Heidelberg. 2009:329–336.

Pierpaoli C, Basser PJ. Toward a quantitative assessment of diffusion anisotropy. Magnetic Resonance in Medicine. 1996; 36:893–906. [PubMed: 8946355]

Raab P, Hattingen E, Franz K, Zanella FE, Lanfermann H. Cerebral Gliomas: Diffusional Kurtosis Imaging Analysis of Microstructural Differences1. Radiology. 2010; 254:876–881. [PubMed: 20089718]

Reese TG, Heid O, Weisskoff RM, Wedeen VJ. Reduction of eddy-current-induced distortion in diffusion MRI using a twice-refocused spin echo. Magnetic Resonance in Medicine. 2003; 49:177–182. [PubMed: 12509835]

Sen PN, Basser PJ. A model for diffusion in white matter in the brain. Biophysical Journal. 2005; 89:2927–2938. [PubMed: 16100258]

Shepherd G, Raastad M. Axonal varicosity distributions along parallel fibers: a new angle on a cerebellar circuit. The Cerebellum. 2003; 2:110–113. [PubMed: 12880178]

Smith SM, Jenkinson M, Johansen-Berg H, Rueckert D, Nichols TE, Mackay CE, Watkins KE, Ciccarelli O, Cader MZ, Matthews PM, Behrens TEJ. Tract-based spatial statistics: Voxelwise analysis of multi-subject diffusion data. Neuroimage. 2006; 31:1487–1505. [PubMed: 16624579]

Stanisz GJ, Kecojevic A, Bronskill MJ, Henkelman RM. Characterizing white matter with magnetization transfer and T2. Magnetic Resonance in Medicine. 1999; 42:1128–1136. [PubMed: 10571935]

Stanisz GJ, Wright GA, Henkelman RM, Szafer A. An analytical model of restricted diffusion in bovine optic nerve. Magnetic Resonance in Medicine. 1997; 37:103–111. [PubMed: 8978638]

Syková E, Nicholson C. Diffusion in Brain Extracellular Space. Physiological Reviews. 2008; 88:1277–1340. [PubMed: 18923183]

Tabesh A, Jensen JH, Ardekani BA, Helpern JA. Estimation of tensors and tensor-derived measures in diffusional kurtosis imaging. Magnetic Resonance in Medicine. 2010 in press.

Tanner JE, Stejskal EO. Restricted Self-Diffusion of Protons in Colloidal Systems by Pulsed-Gradient Spin-Echo Method. Journal of Chemical Physics. 1968; 49:1768–&.

Tang Y, Nyengaard JR, Pakkenberg B, Gundersen HJG. Age-Induced White Matter Changes in the Human Brain: A Stereological Investigation. Neurobiology of Aging. 1997; 18:609–615. [PubMed: 9461058]

Thomason ME, Thompson PM. Diffusion Imaging, White Matter, and Psychopathology. Annu. Rev. Clin. Psycho. 2011; 7 in press.

Tuch D. Q-ball imaging. Magnetic Resonance in Medicine. 2004; 52:1358–1372. [PubMed: 15562495]

Warlop NP, Achten E, Fieremans E, Debruyne J, Vingerhoets G. Transverse diffusivity of cerebral parenchyma predicts visual tracking performance in relapsing-remitting multiple sclerosis. Brain and Cognition. 2009; 71:410–415. [PubMed: 19576672]

Warlop NP, Fieremans E, Achten E, Debruyne J, Vingerhoets G. Callosal function in MS patients with mild and severe callosal damage as reflected by diffusion tensor imaging. Brain Research. 2008; 1226:218–225. [PubMed: 18582444]

Wedeen VJ, Hagmann P, Tseng W-YI, Reese TG, Weisskoff RM. Mapping complex tissue architecture with diffusion spectrum magnetic resonance imaging. Magnetic Resonance in Medicine. 2005; 54:1377–1386. [PubMed: 16247738]

Westin, C.; Maier, S.; Khidhir, B.; Everett, P.; Jolesz, F.; Kikinis, R. Image Processing for Diffusion Tensor Magnetic Resonance Imaging.. In: Taylor, C.; Colchester, A., editors. Medical Image Computing and Computer-Assisted Intervention – MICCAI'99. Springer Berlin; Heidelberg: 1999. p. 441-452.

Highlights

- DKI is a clinically feasible extension of DTI to probe restricted diffusion in tissue

- We provide a physically meaningful interpretation of DKI metrics in white matter

- White matter parameters: intra- and extra-axonal diffusivities, axonal water fraction

- White matter parameters estimated *in vivo* in healthy brain agree with prior knowledge

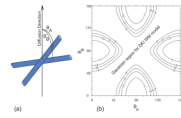- Convenient method for the clinical assessment of white matter in health and disease

Fig. 1.
Illustration of the *b*-value dependence of the criterion of Eq. (**6**) for determining whether the diffusion is effectively Gaussian in an axonal compartment consisting of two crossing fibers oriented at polar angles (θ_A, θ_B) relative to a particular diffusion direction of interest, as illustrated in Fig. 1(a). Depending on the polar angles (shown in degrees), this system can be considered a "Gaussian compartment" when the ($D_a b$) is smaller than the plotted values in Fig. 1(b), with D_a the free intra-axonal diffusivity. The central portion of the plot and the corner regions correspond to the most Gaussian diffusion.
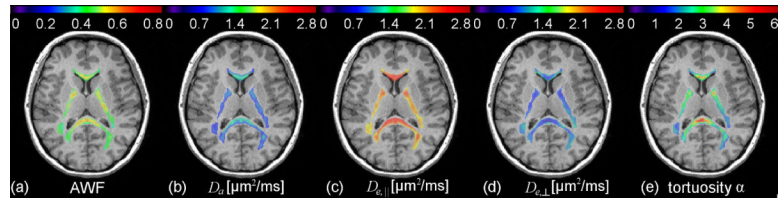
Fig. 2.
WM parametric transversal maps as overlays on the MPRAGE image of a healthy young control: (a) the AWF according to Eq. (**7**); (b) the axonal diffusivity according to Eq. (12); (c) the axial EAS diffusivity according to Eq. (13); (d) the radial EAS diffusivity according to (Eq. (14); (e) the tortuosity of the EAS accordign to Eq. (15). A mask was applied to the parametric maps that selects regions with aligned fibers according to Eq. (16).
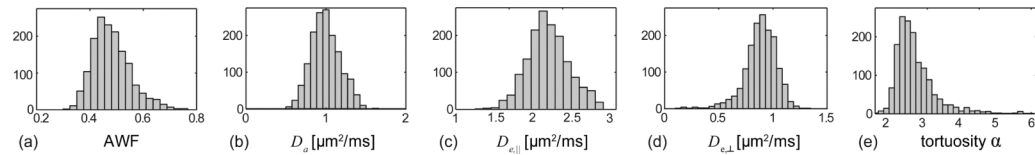
Fig. 3.
Histograms of the WM parameters of a healthy young control over all WM voxels consisting of aligned fibers (according to Eqn. (16)): (a) the AWF according to Eq. (**7**); (b) the axonal diffusivity according to Eq. (12); (c) the axial EAS diffusivity according to (Eq. (13); (d) the radial EAS diffusivity according to Eq. (14); (e) the tortuosity of the EAS according to Eq. (15). The histograms of the other 2 subjects look very similar (not shown here).
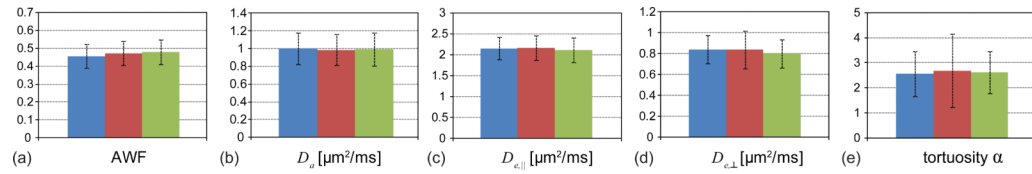
Fig. 4.
Mean values of the WM indices in 3 healthy young adults: (a) the AWF according to Eq. (**7**); (b) the axonal diffusivity according to Eq. (12); (c) the axial EAS diffusivity according to (Eq. (13); (d) the radial EAS diffusivity according to Eq. (14); (e) the tortuosity of the EAS according to Eq. (15). The error bars represent the standard variation for all WM voxels consisting of aligned fibers (mask according to Eqn. (16)).
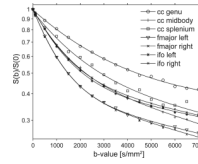
Fig. 5.
The decay of the DWI-signal relative to the $b = 0$ – signal for different fiber bundles with the diffusion gradient applied in the direction perpendicular to the fiber bundle. The solid lines represent the optimal biexponential fits.
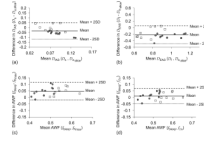
Fig. 6.
Comparison between the parameters obtained from biexponential fitting to high *b*-value diffusion data in the slice direction of the patient coordinate system and the DKI-WM model parameters for ROIs with the main fiber direction parallel to the AC-PC plane. Bland-Altman plots are shown assessing the agreement between: (a) the slow diffusion coefficient, D_s, and IAS diffusivity, $D_{a,slice}$; (b) the fast diffusion coefficient, D_f, and EAS diffusivity, $D_{e,slice}$; (c) the biexponential slow component volume fraction f_{biexp}, and the AWF $f_{K_{max}}$ (Eq. (**7**)); (d) the biexponential slow component volume fraction f_{biexp}, and the AWF f_{ROI} (Eq. (**8**)). In each plot, the mean bias and limits of agreement are indicated by the solid and dashed lines, respectively. The radial EAS diffusivity is lower, and the AWF higher, in the ROIs in the corpus callosum (□) than in the ROIs of the forceps major (●) and inferior occipital fasciculus (●).

Fig. B.1.

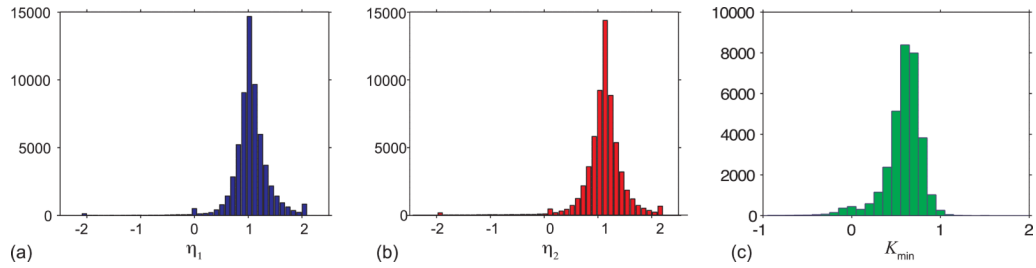Histograms of (a) η_1, and (b) η_2, as defined in Eq. (B.7), and (c) K_{min} (the minimum kurtosis minimum for all directions) over all non-CSF voxels of the brain of a healthy young control. The η-values show a reasonably narrow distribution centered around 1 (with standard deviations SD = 0.3), which corresponds to the upper sign solution of Eqn. (B.3) and (B.4) and indicates that $D_{e,i} \geq D_{a,i}$ in the brain. The finite SD may reflect measurement noise as well as the approximate nature of our model. We also noted negative η-values in a very small number of voxels of the corpus callosum (< 0.2 % of all WM-voxels), but neglected those voxels as the corresponding D_3-values were very small which makes the corresponding kurtosis tensor elements difficult to be determine accurately. The K_{min} values show a distribution of predominantly positive values centered around 0.58 (with standard deviation SD = 0.22), indicating that $D_{e,i} \geq D_{a,i}$ in any frame of reference.